Editors' Suggestion

Unravelling the Surface Local Spin Dynamics in Magnetic Nanoparticles by Means of NMR Relaxometry

M. Basini,[1,2,*] M. Mariani,[3] Q. L. Vuong,[4] Y. Gossuin,[4] S. Slimani,[5,6] G. Singh,[7] D. Peddis,[5,6] and A. Lascialfari[3,8]

[1]Department of Physics, Università degli studi di Milano and INSTM Unit, I-20133 Milano, Italy
[2]Department of Phyisics, ETH Zürich, Auguste-Piccard-Hof 1, 8093 Zürich, Switzerland
[3]Department of Physics, University of Pavia, Via Bassi 6, I-27100 Pavia, Italy
[4]Biomedical Physics Department, University of Mons, B-7000 Mons, Belgium
[5]Department of Chemistry and Industrial Chemistry & Genova, INSTM RU , nM2-Lab, University of Genova, 16146 Genova, Italy
[6]Institute of Structure of Matter, National Research Council, nM2-Lab, Via Salaria km 29.300, Monterotondo Scalo 00015, Roma, Italy
[7]School of Biomedical Engineering, Sydney Nano Institute, The University of Sydney, Sydney 2008, Australia
[8]INFN Pavia Unit, Via Bassi 6, I-27100 Pavia, Italy

(Received 23 January 2025; revised 8 April 2025; accepted 30 April 2025; published 29 May 2025)

We singled out the surface and bulk spin dynamics in magnetic hollow nanoparticles by means of nuclear magnetic resonance relaxometry. Experimental ^{1}H-NMR-dispersion curves (NMR-D), measured across a wide frequency range (10^4 Hz $< f < 3 \times 10^8$ Hz), show the presence of a high-frequency contribution to the longitudinal relaxation rate, evidenced for the first time and ascribed to the surface spin dynamics. The nuclear longitudinal relaxation rates were successfully analyzed by means of a phenomenological model accounting for the two spin populations, i.e., surface and core spins. The fit of the longitudinal NMR-D data by means of this model allowed for the estimation of the hyperfine coupling constant of the surface spins, and of the superparamagnetic $1/\tau_N$ and surface-paramagnetic-like $1/\tau_C^{\mathrm{surf}}$ spin-spin correlation frequency, the last one being larger by more than 1 order of magnitude. These experimental results provide a substantial contribution to the basic knowledge of spin dynamics in nanoscale systems.

DOI: 10.1103/PhysRevLett.134.216703

The electronic spin dynamics in iron oxide magnetic nanoparticles (MNPs) have been quite extensively investigated over the past 25 years [1–9]. However, a complete understanding remains elusive, in particular when surface effects are considered [10–13]. The effect of the spin disorder near the surface in MNPs with "full" magnetic core (FMNPs) is indeed not easy to be detected experimentally, due to the low fraction of surface spins compared to core ones. Moreover, even if an excellent control of the crystallinity and the size distribution has recently been achieved, different synthesis procedures strongly affect the properties and the thickness of the surface spin corona [14]. Some years ago, "hollow" systems were synthesized [15] with the idea to increase the surface to volume ratio, allowing one to enhance the probability to observe the dynamics of surface spins. Despite the interest that the hollow geometry has piqued for unravelling fundamental magnetic dynamics and for possible applications in nanomedicine, sensoristics, magnetic storage, and quantum information [16–20], relatively few studies focused on the hollow magnetic nanoparticles (HMNPs) static and dynamic magnetic properties [21–30]. None have clearly unraveled the surface spin dynamics.

Owing to the time window of the investigated dynamics in nanostructured systems at room temperature (i.e., correlation times of the order 10^{-5}-10^{-12} s), the experimental techniques able to reveal the electronic correlation times should probe frequencies faster than 10^4 Hz. Mossbauer spectroscopy, inelastic neutron scattering, muon spin resonance (μSR), AC magnetometry, and NMR relaxometry are examples of suitable experimental techniques. For instance, ^{1}H NMR can be performed on MNPs solutions in a wide frequency range ($\sim 10^4$–10^9 Hz), thus being able to probe dynamics occurring at different timescales, like, e.g., molecular rotation, diffusion, Néel reversal, and paramagnetic spin reorientation, here included the surface spins dynamics. Remarkably, biomedical applications of aqueous solutions of MNPs utilize NMR and NMR-dispersion (NMR-D) experimental studies of the magnetic spin dynamics for optimizing their therapeutic (e.g., magnetic hyperthermia [15,31]) and diagnostic (MRI [16]) uses

*Present address: Department of Phyisics, ETH Zürich, Auguste-Piccard-Hof 1, 8093 Zürich, Switzerland

in the clinic. Applications of MNPs as sensors, magnetic storage, and quantum information systems have also been realized [14,19,20].

From a fundamental perspective, the required low concentration of MNPs (i.e., [Fe] < 0.5 mmol/l) in such NMR aqueous solutions leads to negligible interparticle interactions, thus allowing a simpler modeling strategy. In more detail, ^{1}H NMR relaxation in the presence of MNPs occurs when the hyperfine dipolar (outersphere model) and/or contact interactions between the ^{1}H nuclear spin and the MNP's electronic spin are modulated by a specific dynamics, whose frequency is resonant with the proton (i.e., hydrogen nucleus) Larmor angular frequency ω_L. Given a Larmor frequency $f_L = \omega_L/2\pi$, in the weak collision approach [32,33] the nuclear longitudinal relaxation rate (i.e., $1/T_1$, also called spin-lattice relaxation rate) is proportional to the spectral density of the electronic spin fluctuations $J(\omega)$ calculated at ω_L. It is widely known that the dynamics of the superparamagnetic electronic spins of FMNPs could be highly efficient in increasing the relaxation rate of the proton magnetization in the solution. Several investigations [34–38], dedicated to dynamical studies on FMNPs by means of ^{1}H-NMR relaxometry, succeeded in revealing an effective correlation time τ_{eff} accounting for the Néel flipping time of the FMNPs' electronic magnetization (i.e., τ_N) and for the Brownian rotation and diffusional time of the nanoparticles in solution. The existing experimental data and theories accounting for FMNPs foresee a strong decrease of $1/T_1$ in the frequency region $f > 10$ MHz, where the density of the electronic spin fluctuations drops down [36].

In the above framework, the contribution to the NMR signal coming from the (bulk water) hydrogen nuclei interacting with the surface spins is generally neglected. In this work, we investigated full and hollow magnetic nanoparticles, comparing their spin dynamics in the range 10^4 Hz $< f < 3 \times 10^8$ Hz. A signature of the surface spin dynamics occurring at $f > 10$–100 MHz is evidenced, to the best of our knowledge, for the first time. Thus we showed the capability of the wide band ^{1}H NMR technique to be sensitive to the surface spin dynamics in MNPs, a largely investigated fundamental problem for decades [1,39,40] and a possible crucial issue for many applications.

A sample composed of a nanosized full maghemite core (FMNP) with diameter d, named F_d, and coated with oleic acid has been synthesized using the well-established protocol proposed by Sun *et al.* [41]. Starting from the FMNP sample, MNPs with HMNPs have been synthesized following a procedure based on the Kirkendall effect [42–50]. Iron pentacarbonyl [Fe(Co)5] was decomposed in a controlled atmosphere at around 220 °C in oleylamine and octadecene [43–51]. The resulting iron-based nanoparticles (NPs) are oxidized at 220 °C in solution by means of oleic acid [44,45]. The hollow topology results from the different self-diffusion velocity of iron and oxygen ions [42,44]. By this synthetic strategy five samples of hollow magnetic nanoparticles characterized by an internal D_{int} and an external D_{ext} diameter and named as H_$D_{\text{int}}/D_{\text{ext}}$, all coated with oleic acid, were obtained. The structural and morphological analysis was performed using x-ray diffraction (XRD) measurements [TT 3003 diffractometer equipped with a secondary graphite monochromator, employing CuKα radiation ($\lambda = 1.5418$ Å)]. Transmission electron microscopy (TEM), performed by a Hitachi S-5500 microscope operating at 30 KV, was utilized for the size and morphological characterization. The static dc magnetization vs temperature (2–300 K, data not reported; see also [21,41,42]) and vs magnetic field (0–7 Tesla) was measured by means of a Quantum Design MPMS-XL7 SQUID magnetometer. The ^{1}H longitudinal relaxation time (T_1) NMR measurements were performed at room temperature by means of the fast-field-cycling (FFC) technique in the range 10 kHz–10 MHz, and by Fourier Transform (FT)-NMR wide band spectrometers in the range 10–300 MHz (magnetic field till 7 Tesla). For measuring T_1 we used the typical saturation $\pi/2$-$\pi/2$ recovery sequence. It is worth noting that the value of the ratio T_2/T_1 ($\sim$1) at the lowest frequency and the zero field cooling-field cooling (ZFC-FC) plus δM curves (data not reported) showed that there is no particle aggregation.

The TEM and superconducting quantum interference device (SQUID) magnetometer results (see [21,45,46] for further details on size distribution) are shown in Fig. 1, where M vs μ_0H curves were collected at room temperature (i.e., T $\approx$ 300 K) on NPs samples dispersed in solution (concentration 3 mMol $<$ c $<$ 35 mMol). From these data [52], we obtained the diameters d, D_{int}, D_{ext}; the bulk superparamagnetic volume V_{SPM}; the saturation magnetization M_s; the blocking temperature T_B; and the total magnetic volume V_{tot}, reported in Table I. It is worth noting

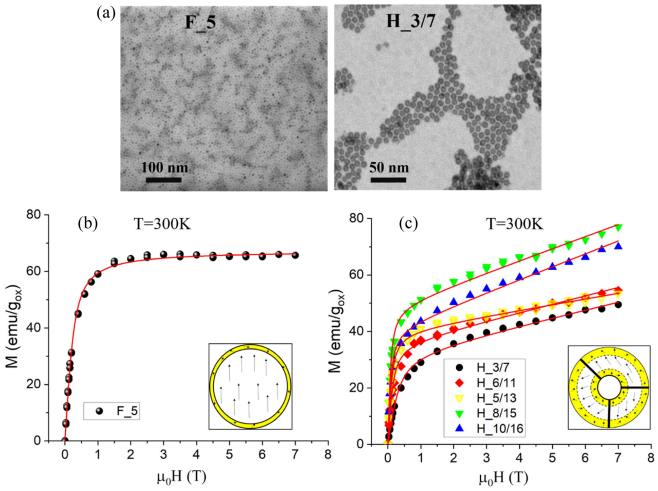

FIG. 1. (a) Example TEM images of full F_5 (left) and hollow H_3/7 (right) samples. (b) Magnetization vs field at room temperature is shown for full (b) and hollow (c) samples in solution, subtracted by the diamagnetic contribution of the solvent and the sample holder. The curve fits discussed in the text are also shown. The experimental data are available here [52].

TABLE I. List of the parameters extracted from TEM images (D_{int}, D_{ext}; V_{tot} is calculated from D_{int} and D_{ext}) and from the fitting of the M vs H curves [Eq. (1)] collected on nanoparticle solutions at room temperature (M_s, V_{SPM}, and χ^{PM}). D_{int} and D_{ext} are the internal and external diameters of the hollow NPs, d is the core diameter of the full NP, V_{tot} is the total magnetic volume, M_s is the saturation magnetization, V_{SPM} is the volume of the part containing superparamagnetic bulk spins [see Eq. (1)], χ_{PM} is the paramagneticlike susceptibility of the surface spin corona, and T_B is the blocking temperature extracted from M_{FC}-M_{ZFC} measured at 2.5 mT [53].

Sample	D_{int} (nm)	D_{ext} or d (nm)	V_{tot} (nm^3)	M_s (emu/$g_{\gamma\text{-Fe2O3}}$)	(V_{SPM}/V_{tot})	χ^{PM} (emu/$g_{\gamma\text{-Fe2O3}}$ Tesla)	T_B (K)
F_5	⋯	5(0.3)	65(8)	66(4)	0.92	0(0.1)	14(5)
H_3/7	2.8(0.3)	7.4(0.3)	200(15)	31(2)	0.64	2.7(0.3)	16(5)
H_6/12	6.0(0.2)	12.0(0.3)	791(30)	35(2)	0.48	2.9(0.5)	56(5)
H_5/13	5.0(0.2)	13.0(0.3)	1084(21)	41(2)	0.69	1.9(0.4)	81(5)
H_8/15	8.3(0.4)	15.0(0.5)	1467(53)	47(3)	0.66	4.0(0.5)	49(5)
H_10/16	10.0(0.4)	16.0(0.4)	1620(32)	40(2)	0.42	4.6(0.5)	60(5)

that all the magnetic measurements were performed on the same solutions used in the NMR investigation.

The reference sample F_5 (full, d = 5 nm) displays superparamagnetic behavior at room temperature (i.e., H_c and $M_r \approx 0$), with saturation magnetization $M_s \simeq 66$ emu/$g_{\gamma\text{-Fe2O3}}$ [Fig. 1(b)]. On the other hand, all the M vs H curves of HMNPs display an additional linear contribution [Fig. 1(c)] which prevents the magnetization from reaching saturation even at very high fields. The linear contribution was first observed by Cabot [21] and ascribed to the spins at the shell surface and crystallite interfaces, which are strongly pinned along local axes due to surface anisotropy. Following the idea of two independent spin populations as proposed in Refs. [21–23,47,54] we fitted the experimental data of Fig. 2 by means of a linear combination of a Langevin function accounting for the bulk superparamagnetic spins, and a linear contribution accounting for the surface paramagnetic spins:

$$M(H) = M_s L\left(\frac{M_s V_{SPM}\mu_0 H}{k_B T}\right) + \chi^{PM} H, \qquad (1)$$

where k_B is the Boltzmann constant, $V_{SPM}(\leq V_{tot})$ is the volume corresponding to the bulk core spins, and χ^{PM} is the paramagnetic (PM)-like susceptibility of the surface spin corona. The fitting results are shown as red solid curves in Fig. 1 with the values of the main fitting parameters, i.e., M_s, V_{SPM}, and χ^{PM}, listed in Table I, together with the blocking temperature T_B, extracted from ZFC-FC curves recorded at 2.5 mT (data not shown). For all HMNPs, V_{SPM} was found proportional to the extracted value of M_s, which is consistently smaller than 50 emu/$g_{\gamma\text{-Fe2O3}}$. This value is lower than that observed in full nanoparticles (FMNPs) of similar size or in bulk maghemite (i.e., 76 emu/$g_{\gamma\text{-Fe2O3}}$ [55]). Additionally, it is worth observing that the response of the surface spin to an external and static magnetic field is well described by a PM-like susceptibility, whose value is an indication of the degree of the frustration at the surface (i.e., higher χ^{PM} indicated higher frustration [15]). Among the investigated samples, we note that H_5/13 displays lower χ^{PM}, thus indicating a lower number of surface spins. The evidence is in line with the observation of a thicker shell for H_5/13 (i.e., 4 nm thick) compared to other samples, as a thicker shell typically hosts larger crystallites and fewer surface spins.

Since the magnetization measurements allowed a clear observation of the surface spins' effect on static magnetic properties, to single out the dynamical effects we performed ^{1}H-NMR relaxation measurements. As already pointed out, these measurements allow one to access spin dynamics frequencies in the range 10^4–3×10^8 Hz. The experimental ^{1}H-NMR D profiles of the nuclear longitudinal "*effective*" *relaxation rate* of our samples, i.e., subtracted by the longitudinal relaxation rate of the bare solvent [$Effective\ relaxation\ rate = (1/T_1) = (1/T_{1,NP+sol}) - (1/T_{1,sol})$, where $(1/T_{1,NP+sol})$ and $(1/T_{1,sol})$ are the longitudinal relaxation rates of the nanoparticle solution and of the bare solvent, respectively], versus the Larmor frequency ν_L for both full and hollow samples are shown as full circles in Fig. 2 (the experimental data are available here [52]).

For superparamagnetic full core nanoparticles (with d < 20 nm), the nuclear longitudinal *effective* relaxation rate (from now on for brevity: longitudinal relaxation rate) the profile is generally explained using the Roch model [56] or its alternatives [38,56–58]. By focusing on the model of Ref. [56], we recall that the longitudinal relaxation rate is described by the equation

$$\frac{1}{T_1^{SPM}} = \frac{32\pi}{135000}\mu_{SPM}^2\gamma_I^2\left(\frac{N_A C}{rD}\right)\left\{7P\frac{L(x)}{x}J^F(\omega_S,\tau_D,\tau_N) + \left[7(1-P)\frac{L(x)}{x} + 3\left(1 - L^2(x) - \frac{2L(x)}{x}\right)\right] \times J^F(\omega_I,\tau_D,\tau_N) + 3L^2(x)J^A\left(\sqrt{2\omega_I\tau_D}\right)\right\}, \qquad (2)$$

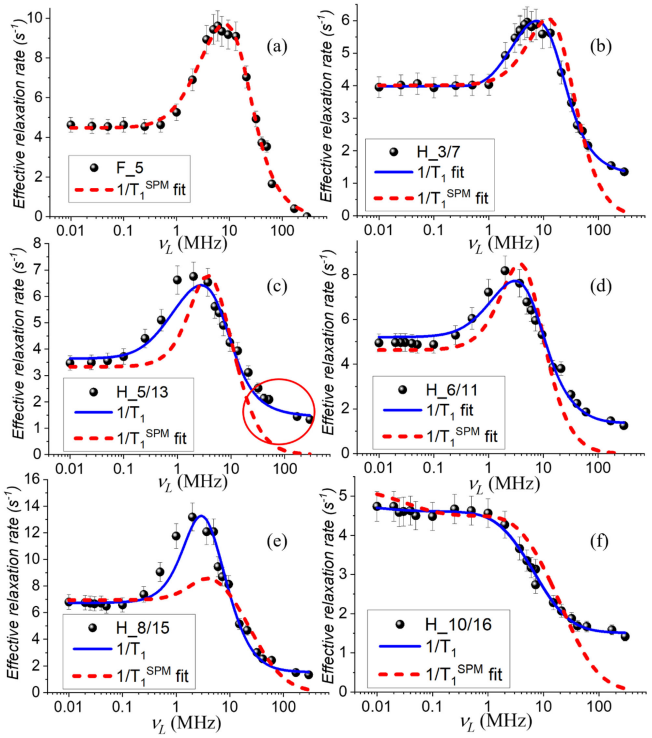

FIG. 2. Experimental NMR D curves (black circles) for the different investigated samples [52]. The red dashed lines represent the best fitting curves by means of Roch's model. The blue lines describe the proposed heuristic model (see main text), which includes the surface spin contribution. The discrepancy obtained in the high field region between the Roch's model and our proposed fitting model is evidenced as an example by the red circle in Fig. (c). The iron concentration in the measured solution (a)–(f) are 0.75 mmol, 4 mmol, 0.75 mmol, 1.68 mmol, 1.18 mmol, 2.77 mmol respectively.

where γ_S, γ_I are the gyromagnetic ratio of electron and proton respectively, μ_{SPM} = total magnetic moment of the superparamagnetic (SPM), spins, N_A = Avogadro number, $L(x)$ is the Langevin function, as defined in Eq. (1), where $x = (\mathrm{M_s}V_{\mathrm{SPM}}\mu_0\mathrm{H}/k_B\mathrm{T})$, C = nanoparticles concentration in Mol/l, D = water translational diffusion coefficient, r = minimum approach distance of the protons to the nanoparticle, τ_D = diffusion correlation time, τ_N = Neél reversal time, ω_I and ω_S are the proton and the electron Larmor frequency respectively, P is an empirical parameter in the Roch model whose value is 1 when the magnetic anisotropy is maximum, and J^A and J^F are the Ayant and Freed spectral function, respectively. J^A and J^F account for the low and high field inflection points of the NMR-D profile, respectively. It is worth noting that the Ayant function inflection occurs at $\omega_I\tau_D \sim 1$ (see Fig. 3). At intermediate fields the relaxation rates are a combination of the high and low field contributions weighted by factors depending on the Langevin function. At high fields the Freed spectral density function $J^F(\omega, \tau_D, \tau_N)$ shows an inflection at $\omega_I\tau_C^{\mathrm{Core}} \sim 1$ (where $1/\tau_C^{\mathrm{Core}} = \tau_D^{-1} + \tau_N^{-1}$). The Ayant function is the limit of the Freed function when $\omega\tau_N \gg 1$.

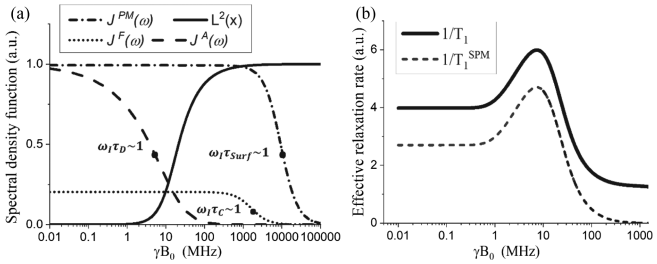

FIG. 3. (a) Different contributions to the longitudinal proton relaxation: the Freed $J^F(\omega)$ and Ayant $J^A(\omega)$ spectral density functions, the squared Langevin function $\mathrm{L}^2(\mathrm{x})$, and the BPP function $J^{\mathrm{PM}}(\omega)$ accounting for the surface, the last one introduced in the present work. (b) *Effective longitudinal relaxation rate* $1/T_1$ (see main text) vs field (NMR (D) as predicted from our phenomenological model accounting for the superparamagnetic "bulk" ($1/T_1^{\mathrm{SPM}}$), and for the total relaxation ($1/T_1$) which includes the paramagneticlike surface spins.

Referring to the longitudinal relaxation rate deduced from the Roch model as $1/T_1^{\mathrm{SPM}}$, from Fig. 2 (where $1/T_1^{\mathrm{SPM}}$ is reported as a dashed red line) one observes that (i) the FMNP profile can be fitted by simply using Eq. (2) and (ii) the HMNP is not fitted by Eq. (2), particularly for what concerns the peak shape and the high fields data.

As HMNP profiles cannot be fitted by Eq. (2), we propose a novel phenomenological model that includes the surface spin contribution, which is not taken into account in previously reported literature [39–51,54]. The spins of the inner and outer surfaces constitute a disordered layer on the nanoparticle boundary that can be thought of as a spherical corona (see yellow area in Fig. 1), with a certain thickness, that can be evaluated by means of Mossbauer spectroscopy under an intense magnetic field [29]. Owing to their lower coordination, the surface spins are expected to flip along the easy axes' directions faster than the "core" ones. Their faster dynamics would contribute to the longitudinal ^{1}H relaxation at high frequency, where the "core" superparamagnetic contribution is low. Thus, for $\omega_L >$ 10–100 MHz the surface spins contribution is expected to dominate the HMNP nuclear relaxation rate.

Based on the proposed model, the ^{1}H NMR $1/T_1$ relaxation rate of the HMNPs samples can be described as a linear combination of a paramagnetic contribution $1/T_1^{\mathrm{PM}}$, from the interaction of the ^{1}H nuclei with the surface spins, and a $1/T_1^{\mathrm{SPM}}$ relaxation [56] associated with the spins of the magnetic core, Eq. (2). The PM surface spin contribution was modeled using a Bloembergen-Purcell-Pound (BPP)-like function, as largely suggested by literature on paramagnetic systems [32–37]. Thus, the *longitudinal* relaxation rate $1/T_1$ for the hollow systems can be written as

$$\frac{1}{T_1} = \frac{1}{T_1^{\mathrm{SPM}}} + \frac{1}{T_1^{\mathrm{PM}}} = \frac{1}{T_1^{\mathrm{SPM}}} + \chi^{\mathrm{PM}}T \times \tilde{A}(N_A C)\frac{\tau_c^{\mathrm{Surf}}}{1+\omega^2(\tau_c^{\mathrm{Surf}})^2} \tag{3}$$

where χ^{PM} is the magnetic susceptibility, T is the temperature, $\tilde{A}$ is the geometrical hyperfine constant [59–61], and τ_c^{Surf} is the surface effective correlation time representing the flipping time of the surface spins. At a first approximation, in the picture described by Eq. (3), the surface PM spins and the core SPM spins act independently, a hypothesis justified by the small number of core and surface spins that interact.

Fig. 3(a) illustrates the frequency dependence of the primary contributions to $(1/T_1^{\mathrm{SPM}})$, i.e., the Freed $J^F(\omega)$ function, the Ayant $J^A(\omega)$ function, the Langevin L(x) contribution, and of the spectral density $J^{\mathrm{PM}}(\omega)$ that accounts for the surface spins. Figure 3(b) represents the expected frequency dependence of $1/T_1$ and $1/T_1^{\mathrm{SPM}}$; see Eq. (3).

We fitted the experimental data of Fig. 2 by means of Eq. (3) fixing in the $(1/T_1)$ expression some physical quantities obtained from the DC magnetic measurements, i.e., the saturation magnetization $\mathrm{M_s}$, the volume of the bulk superparamagnetic core V_{SPM} and the paramagnetic-like χ^{PM}. If we define the effective core spin correlation frequency as $1/\tau_C^{\mathrm{core}} = 1/\tau_N + 1/\tau_D$ (neglecting the Brownian relaxation rate $1/\tau_B$), the free parameters are the Neel time τ_N, the correlation time τ_c^{Surf} of the surface spins, and the hyperfine constant $\tilde{A}$. The blue lines of Fig. 2 represent the best fitting curves. As one can easily see, the agreement with the experimental data significantly improves the early fitting done by the simple Roch's model (red line). In fact, we were able to reproduce not only the low frequency dispersion and the position of the maxima but also the increased high frequency (i.e., > 100 MHz) contribution to the relaxation. Remarkably, the agreement at high frequencies can be ascribed to the surface spins' PM component [second term in Eq. (3)]. In Table II the results of the fit are reported.

From Table II it can be noticed first that τ_N is in the typical range of SPM materials. Instead, the effective correlation time τ_C^{Surf} accounts for a faster dynamics, consistently with the picture of low coordinated and highly disordered surface spins with respect to the core ones. For the H_10/16 sample, the surface spin contribution is dominant, as expected from characterization data, Fig. 1, and Table I. It is important to remark that, even if experimentally we reached a high external applied field corresponding to a relatively high frequency $\nu_{\mathrm{L}} = 300$ MHz, our frequency window was not enough wide to observe on the experimental data the inflection point of $J^{PM}(\omega)$ expected at frequency $\omega_c^{\mathrm{Surf}} = 1/\tau_C^{\mathrm{Surf}}$. One should notice that τ_C^{Surf} is not only defining the dispersion, but also the amplitude of the dispersion, thus allowing for an estimation of this parameter. The estimated value for $1/\tau_C^{\mathrm{Surf}}$ has here to be considered as a lower limit for the frequency of the surface spin fluctuations.

TABLE II. Parameters extracted from the fit of the experimental NMR-D curves of FMNPs and HMNPs by means of Eq. (3). τ_N = Neél flipping time of the superparamagnetic spins, τ_C^{Surf} = surface effective correlation time, χ^{PM} is the paramagnetic susceptibility, T is the temperature, $\tilde{A}$ is the geometrical hyperfine constant.

Sample	τ_N (10^{-9} s)	τ_C^{Surf} (10^{-11} s)	$\chi_{\mathrm{PM}} T \cdot \tilde{A}$ (10^{11} rad^2 s^{-2})
F_5	0.2 (0.1)	⋯	
H_3/7	0.6(0.1)	3.4 (0.7)	0.5(0.1)
H_6/12	2.6(0.5)	2.0(1.2)	2.5(0.6)
H_5/13	1.4(0.6)	5.5(2.2)	1.8(0.5)
H_8/15	3.5(0.7)	4.3(1.5)	3.0(0.8)
H_10/16	25(9)	2.9(1.2)	0.6(0.1)

As seen from column 3 of Table II, the PM nuclear-electron hyperfine coupling $\chi^{\mathrm{PM}} T \cdot \tilde{A}$ is in the typical range of paramagnetic substances previously studied in the literature [21,59,62].

In conclusion, we provided experimental evidence of the surface spin dynamics in magnetic nanoparticles with hollow geometry, revealed by ^{1}H-NMR relaxometry data. These data were fitted using a phenomenological model of the nuclear spin-lattice relaxation rate $(1/T_1)$, whose expression contains two contributions, one from core spins and the other from surface spins. In this model, at room temperature the nanoparticle surface spins were described as an independent paramagneticlike population, with a dynamics more than 1 order of magnitude ($\tau_C^{\mathrm{Surf}} \sim 10^{-11}$ s) faster than the one of the core spins (Néel correlation time $\tau_C^N \sim 10^{-9}$ s). Future planned studies of $(1/T_1)$ vs temperature could confirm the existence and magnitude of the correlation time τ_C^{Surf}, by detecting the surface spins freezing through the observation of a very low temperature ($T < 20$–30 K) anomaly expected when $\tau_c^{\mathrm{Surf}} \cdot \omega_L \approx 1$ (see, e.g., [34]). By means of our findings, we demonstrated the capability of ^{1}H NMR relaxometry to single out different correlation times in a system composed by more than one electronic spin reservoir, and to contribute understanding the fundamental mechanisms of magnetic dynamics in nanoscale systems. Applications of our findings can also be envisaged in different fields, like, e.g., biomedicine, environment, magnetic data storage, sensoristics, and quantum information.

Acknowledgments—M. B. acknowledges the SNSF Ambizione Project No. PZ00P2_216089. A. L. and M. M. acknowledge the INFN MATHER3D research project. A. L. thanks the MIUR Dipartimenti di Eccellenza 2018-2022 Project No. F11I18000680001. The COST action EURELAX No. CA15209 is also acknowledged.

Data availability—The data that support the findings of this article are openly available [52].

[1] G. Schmid, *Nanoparticles: From Theory to Application* (Wiley-VCH, Weinheim, 2004); K. J. Klabunde, *Nanoscale Materials in Chemistry* (Wiley-Interscience, New York, 2001).

[2] A. Fraile Rodríguez, A. Kleibert, J. Bansmann, A. Voitkans, L. J. Heyderman, and F. Nolting, Size-dependent spin structures in iron nanoparticles, Phys. Rev. Lett. **104**, 127201 (2010).

[3] M. M. van Oene, L. E. Dickinson, F. Pedaci, M. Köber, D. Dulin, J. Lipfert, and N. H. Dekker, Biological magnetometry: Torque on superparamagnetic beads in magnetic fields, Phys. Rev. Lett. **114**, 218301 (2015).

[4] H. Liu and C. Di Valentin, Shaping magnetite nanoparticles from first principles, Phys. Rev. Lett. **123**, 186101 (2019).

[5] L. G. Vivas, R. Yanes, D. Berkov, S. Erokhin, M. Bersweiler, D. Honecker, P. Bender, and A. Michels, Toward understanding complex spin textures in nanoparticles by magnetic neutron scattering, Phys. Rev. Lett. **125**, 117201 (2020).

[6] S. Paul, G. Kotagiri, R. Ganguly, A. Subramanian, H. Courtois, C. B. Winkelmann, and A. K. Gupta, Magnetization reversal across multiple serial barriers in a single Fe_3O_4 nanoparticle, Phys. Rev. B **105**, L180410 (2022).

[7] J. Rackham, B. Pratt, D. Griner, D. Smith, Y. Cai, R. G. Harrison, A. Reid, J. Kortright, M. K. Transtrum, and K. Chesnel, Field-dependent nanospin ordering in monolayers of Fe_3O_4 nanoparticles throughout the superparamagnetic blocking transition, Phys. Rev. B **108**, 104415 (2023).

[8] F. L. Durhuus, M. Beleggia, and C. Frandsen, Magnetic and viscous dynamics of spheroidal nanoparticles, Phys. Rev. B **110**, 144425 (2024).

[9] L. Gragnaniello, T. Ma, G. Barcaro, L. Sementa, F. R. Negreiros, A. Fortunelli, S. Surnev, and F. P. Netzer, Ordered arrays of size-selected oxide nanoparticles, Phys. Rev. Lett. **108**, 195507 (2012).

[10] D. A. Garanin and H. Kachkachi, Surface contribution to the anisotropy of magnetic nanoparticles, Phys. Rev. Lett. **90**, 065504 (2003).

[11] A. Kovács, K. Sato, V. K. Lazarov, P. L. Galindo, T. J. Konno, and Y. Hirotsu, Direct observation of a surface induced disordering process in magnetic nanoparticles, Phys. Rev. Lett. **103**, 115703 (2009).

[12] R. E. Camley, R. Macêdo, and K. L. Livesey, Curie-Weiss behavior and the interaction temperature of magnetic nanoparticle ensembles: Local structure strongly affects the magnetic behavior, Phys. Rev. B **110**, 144440 (2024).

[13] P. Sobieszczyk and M. Krupinski, Surface effects in ferrimagnetic TbFe rare-earth–transition-metal thin films and nanoparticles, Phys. Rev. B **109**, 024412 (2024).

[14] A. Ali, T. Shah, R. Ullah, P. Zhou, M. Guo, M. Ovais, Z. Tan, and Y. Rui, Review on recent progress in magnetic nanoparticles: Synthesis, characterization, and diverse applications, Front. Chem. **9**, 629054 (2021).

[15] A. Cabot, V. F. Puntes, E. Shevchenko, Y. Yin, L. Balcells, M. A. Marcus. S. M. Hughes, and A. P. Alivisatos, Vacancy coalescence during oxidation of iron nanoparticles, J. Am. Chem. Soc. **129**, 10358 (2007).

[16] S. V. Spirou, M. Basini, A. Lascialfari, C. Sangregorio, and C. Innocenti, Magnetic hyperthermia and radiation therapy: Radiobiological principles and current practice, Nanomater. Nanotechnol. **8**, 401 (2018).

[17] A. Ghazali and J.-C. Lévy, Two-dimensional arrangements of magnetic nanoparticles, Phys. Rev. B **67**, 064409 (2003).

[18] L. H. F. Andrade, A. Laraoui, M. Vomir, D. Muller, J.-P. Stoquert, C. Estourne's, E. Beaurepaire, and J.-Y. Bigot, Damped precession of the magnetization vector of superparamagnetic nanoparticles excited by femtosecond optical pulses, Phys. Rev. Lett. **97**, 127401 (2006).

[19] T. Neuman, D. S. Wang, and P. Narang, Nanomagnonic cavities for strong spin-magnon coupling and magnon-mediated spin-spin interactions, Phys. Rev. Lett. **125**, 247702 (2020).

[20] K. Konwar, S. Datta Kaushik, D. Sen, and P. Deb, Dynamic spin freezing and magnetic memory effect in ensembles of interacting anisotropic magnetic nanoparticles, Phys. Rev. B **102**, 174449 (2020).

[21] M. Basini, S. Sanna, T. Orlando, L. Bordonali, M. Cobianchi, P. Arosio, M. Mariani, D. Peddis, V. Bonanni, R. Mathieu, T. Kalaivani, G. Singh, J. Larionova, Y. Guari, L. Lartigue, and A. Lascialfari, Low-temperature anomalies in muon spin relaxation of solid and hollow γ-Fe_2O_3 nanoparticles: A pathway to detect unusual local spin dynamics, Phys. Rev. B **102**, 195424 (2020).

[22] A. Cabot, A. P. Alivisatos, V. F. Puntes, L. Balcells, O. Iglesias, and A. Labarta, Magnetic domains and surface effects in hollow maghemite nanoparticles, Phys. Rev. B **79**, 094419 (2009).

[23] H. Khurshid, P. L. Kelley, Ò. Iglesias, J. Alonso, M. H. Phan, C. J. Sun, M. L. Saboungi, and H. Srikanth, Spin-glass-like freezing of inner and outer surface layers in hollow γ-Fe_2O_3 nanoparticles, Sci. Rep. **5**, 15054 (2015).

[24] D. Thapa, V. R. Palkar, M. B. Kurup, and S. K. Malik, Properties of magnetite nanoparticles synthesized through a novel chemical route, Mater. Lett. **58**, 2692 (2004).

[25] Q. Li, C. W. Kartikowati, S. Horie, T. Ogi, T. Iwaki, and K. Okuyama, Correlation between particle size/domain structure and magnetic properties of highly crystalline Fe_2O_3 nanoparticles, Sci. Rep. **7**, 9894 (2017); M. S. Andersson, R. Mathieu, P. S. Normile, S. S. Lee, G. Singh, P. Nordblad, and J. A. De Toro, Magnetic properties of nanoparticle compacts with controlled broadening of the particle size distribution, Phys. Rev. B **95**, 184431 (2017).

[26] T. N. Shendruk, R. D. Desautels, B. W. Southern, and J. van Lierop, The effect of surface spin disorder on the magnetism of γ-Fe_2O_3 nanoparticle dispersions, Nanotechnology **18**, 455704 (2007).

[27] D. S. Negi, H. Sharona, U. Bhat, S. Palchoudhury, A. Gupta, and R. Datta, Surface spin canting in Fe_3O_4 and $CoFe_2O_3$ nanoparticles probed by high-resolution electron energy loss spectroscopy, Phys. Rev. B **95**, 174444 (2017).

[28] M. Anand, J. Carrey, and V. Banerjee, Spin morphologies and heat dissipation in spherical assemblies of magnetic nanoparticles, Phys. Rev. B **94**, 094425 (2016).

[29] F. Sayed, N. Yaacoub, Y. Labaye, R. Sayed Hassan, G. Singh, P. Anil Kumar, J. M. Greneche, R. Mathieu, G. C. Hadjipanayis, E. Agostinelli, and D. Peddis, Surface effects in ultrathin iron oxide hollow nanoparticles: Exploring magnetic disorder at the nanoscale, J. Phys. Chem. C **122**, 7516 (2016).

[30] V. Bonanni, M. Basini, D. Peddis, A. Lascialfari, G. Rossi, and P. Torelli, X-ray magnetic circular dichroism discloses surface spins correlation in maghemite hollow nanoparticles, Appl. Phys. Lett. **112**, 022404 (2018).

[31] S. V. Spirou, M. Basini, A. Lascialfari, C. Sangregorio, and C. Innocenti, Magnetic hyperthermia and radiation therapy: Radiobiological principles and current practice, Nanomater. Nanotechnol. **8**, 401 (2018).

[32] C. P. Slichter, *Principles of Magnetic Resonance*, 3rd edition (Springer-Verlag, New York, 1990); I. Bertini and C. Luchinat, NMR of paramagnetic substances in coord, Chem. Rev. **150**, 1 (1996).

[33] T. Moriya, Nuclear magnetic relaxation in antiferromagnetics, Prog. Theor. Phys. **16**, 23 (1956); T. Moriya, Nuclear magnetic relaxation near the Curie temperature, Prog. Theor. Phys. **28**, 371 (1962).

[34] T. Orlando, A. Capozzi, E. Umut, L. Bordonali, M. Mariani, P. Galinetto, F. Pineider, C. Innocenti, P. Masala, F. Tabak, M. Scavini, P. Santini, M. Corti, C. Sangregorio, P. Ghigna, and A. Lascialfari, Spin dynamics in hybrid iron oxide–gold nanostructures, J. Phys. Chem. C **119**, 1224 (2015).

[35] M. Basini, T. Orlando, P. Arosio, M. F. Casula, D. Espa, S. Murgia, C. Sangregorio, C. Innocenti, and A. Lascialfari, Local spin dynamics of iron oxide magnetic nanoparticles dispersed in different solvents with variable size and shape: A ^{1}H NMR study, J. Chem. Phys. **146**, 034703 (2017).

[36] Y. Gossuin, T. Orlando, M. Basini, D. Henrard, A. Lascialfari, C. Mattea, S Stapf, and Q. L. Vuong, NMR relaxation induced by iron oxide particles, Nanotechnology **27**, 155706 (2016).

[37] L. Bordonali, Y. Furukawa, M. Kraken, F. J. Litterst, C. Sangregorio, M. F. Casula, and A. Lascialfari, ^{1}H-NMR study of the spin dynamics of fine superparamagnetic nanoparticles, Phys. Rev. B **85**, 174426 (2012).

[38] M. Lévy, F. Gazeau, C. Wilhelm, S. Neveu, M. Devaud, and P. Levitz, Revisiting MRI contrast properties of nanoparticles: Beyond the superparamagnetic regime, J. Phys. Chem. C **117**, 15369 (2013).

[39] J. L. Dormann, D. Fiorani, and E. Tronc, *Magnetic Relaxation in Fine Particle Systems*, Advances of Chemical Physics Vol. 98 (Wiley, New York, 1997), p. 283.

[40] Y. Xie, J. Li, Z. Penga, Y. Yao, and S. Chena, A first-principle study on the atomic-level mechanism of surface effect in nanoparticles, Mater. Today Commun. **24**, 100948 (2020).

[41] C. Sun, J. S. H. Lee, and M. Zang, Magnetic nanoparticles in MR imaging and drug delivery, Adv. Drug Delivery Rev. **60**, 1252 (2008).

[42] Y. Yin, R. M. Rioux, C. K. Erdonmez, S. Hughes, G. Somorjai, and A. P. Alivisatos, Formation of hollow nanocrystals through the nanoscale Kirkendall effect, Science **304**, 711 (2004).

[43] H. J. Fan, U. Gsele, and M. Zacharias, Formation of nanotubes and hollow nanoparticles based on Kirkendall and diffusion processes: A review, Small **3**, 1660 (2007).

[44] V. Bonanni, M. Basini, D. Peddis, A. Lascialfari, G. Rossi, and P. Torelli, X-ray magnetic circular dichroism discloses surface spins correlation in maghemite hollow nanoparticles, Appl. Phys. Lett. **112**, 022404 (2018).

[45] M. Basini, Effect of the hollow topology on the sin dynamics in iron oxide magnetic nanoparticles, Ph.D. thesis, Università degli Studi di Milano, 2017.

[46] M. Basini *et al.*, Low-temperature anomalies in muon spin relaxation of solid and hollow γ-Fe_2O_3 nanoparticles: A pathway to detect unusual local spin dynamics nanoparticle, Phys. Rev. B **105**, 195424 (2020); see Supplemental Material at https://link.aps.org/supplemental/10.1103/PhysRevB.102.195424 for sample characterization of size, morphology, and magnetic state.

[47] H. Khurshid, W. Li, V. Tzitzios, and G. C. Hadjipanayis, Chemically synthesized hollow nanostructures in iron oxides, Nanotechnology **22**, 265605 (2011).

[48] F. Sayed, Hollow magnetic nanoparticles: Experimental and numerical studies, Ph.D. thesis, L'Université du Maine et L'Ecole Doctorale des Sciences et Technologie, 2016.

[49] I. J. Bruvera, P. M. Zelis, M. P. Calatayud, G. F. Goya, and F. H. Sanchez, Determination of the blocking temperature of magnetic nanoparticles: The good, the bad, and the ugly, J. Appl. Phys. **118**, 184304 (2015).

[50] C. Cannas, A. Musinu, G. Piccaluga, D. Fiorani, D. Peddis, H. K. Rasmussen, and S. Mørup, Magnetic properties of cobalt ferrite–silica nanocomposites prepared by a sol-gel autocombustion technique, J. Chem. Phys. **125**, 164714 (2006).

[51] X. Batlle and A. Labarta, Finite-size effects in fine particles: Magnetic and transport properties, J. Phys. D **35**, R15 (2002).

[52] Dataset for: Unravelling the surface local spin dynamics in magnetic nanoparticles by means of NMR Relaxometry, 10.3929/ethz-b-000733411.

[53] D. Peddis, M. T. Qureshi, S. H. Baker, C. Binns, M. Roy, S. Laureti, D. Fiornai, P. Nordblad, and R. Mathieu, Magnetic anisotropy and magnetization dynamics of Fe nanoparticles embedded in Cr and Ag matrices, Philos. Mag. **95**, 3798 (2015).

[54] Y. Gossuin, S. Disch, Q. L. Vuong, P. Gillis, R. P. Hermann, J.-H. Park, and M. J. Sailor, NMR relaxation and magnetic properties of superparamagnetic nanoworms, Contrast Media Mol. Imaging **5**, 318 (2010).

[55] C. J. Goss, Saturation magnetisation, coercivity and lattice parameter changes in the system Fe_3O_4-γFe_2O_3, and their relationship to structure, Phys. Chem. Miner. **16**, 164 (1988).

[56] A. Roch, R. N. Muller, and P. Gillis, Theory of proton relaxation induced by superparamagnetic particles, J. Chem. Phys. **110**, 5403 (1999).

[57] M. Lévy, C. Wilhelm, M. Devaud, P. Levitz, and F. Gazeau, How cellular processing of superparamagnetic nanoparticles affects their magnetic behavior and NMR relaxivity: Magnetic and nmr behaviors of cell-processed USPIO, Contrast Media Mol. Imaging **7**, 373 (2012).

[58] S. Laurent, D. Forge, M. Port, A. Roch, C. Robic, L. Vander Elst, and R. N. Muller, Magnetic iron oxide nanoparticles: Synthesis, stabilization, vectorization, physicochemical characterizations, and biological applications, Chem. Rev. **108**, 2064 (2008).

[59] J. Tejada, R. D. Zysler, E. Molins, and E. M. Chudnovsky, Evidence for quantization of mechanical rotation of magnetic nanoparticles, Phys. Rev. Lett. **104**, 027202 (2010).

[60] A. Sukhov and J. Berakdar, Local control of ultrafast dynamics of magnetic nanoparticles, Phys. Rev. Lett. **102**, 057204 (2009).

[61] F. Borsa, A. Lascialfari, and Y. Furukawa, NMR in magnetic molecular rings and clusters, in *Novel NMR and EPR Techniques*, edited by J. Dolinŝek, M. Vilfan, and S. Žumer, Lecture Notes in Physics, Vol. 684 (Springer, Berlin, Heidelberg, 2006).

[62] F. Borsa and A. Rigamonti, *Magnetic Resonance of Phase Transitions* (Academic, New York, 1979).